29th International Cosmic Ray Conference Pune (2005) **00**, 101–104

Three dimensional propagation of secondary antiprotons in the atmosphere

S.A. Stephens[a]
(a) Tata Institute of Fundamental Research, Homi Bhabha Road, Mumbai 400 005, India
Presenter: S.A. Stephens(melodena@msn.com), ind-stephens-A-abs1-og13-oral

Three dimensional propagation of secondary antiproton ($\bar{p}$) in the atmosphere is undertaken to examine the change of spectral shape of $\bar{p}$ with atmospheric depth. This has been carried out numerically by solving simultaneously the propagation equations of $\bar{p}$ and $\bar{n}$ at different zenith angles. 3-D effect comes from the angular distribution of $\bar{p}$s produced in high energy interactions [1] and the important one being the tertiary production from deep inelastic collisions of $\bar{p}$s. This involves the energy distribution of tertiary $\bar{p}$, its transverse momentum, the consequent direction of the interacting $\bar{p}$ with respect to it and the rotation of this angle in the azimuthal plane. The assumptions involved and the procedure are described in this article and the results are discussed in comparison with the available data in the atmosphere.

1. Introduction

Determination of the secondary antiproton spectrum in the atmosphere is very essential to establish the exact nature of the primary spectrum measured using balloon borne detectors. The production spectrum of $\bar{p}$s peaks around 2 GeV and due to propagation in the atmosphere, this spectral peak shifts to lower energies and the low energy spectrum is considerably modified due to ionization loss and by deep inelastic interaction, which produces tertiary $\bar{p}$ [1]. Theoretical calculations were carried out both by analytical [1] and Monte Carlo methods [2]. In these investigations the tertiary $\bar{p}$ is assumed to move in the direction of the interacting $\bar{p}$, which simplifies the calculation to a large extent. Stephens [1] assumed that $\sigma_{deepin}(E)$ in $(\bar{p}, p)$ interactions is identical to that for (p, p),while others used the difference between the total cross-section and the sum of elastic and annihilation cross-sections, $\sigma_{in}^{T}(\bar{p}, p) = \sigma_{T}(\bar{p}, p) - [\sigma_{el}(\bar{p}, p) - \sigma_{an}(\bar{p}, p)]$. $\sigma_{in}^{T}(\bar{p}, p)$ includes charge exchange process $\bar{p} + p \rightarrow \bar{n} + n$ at low energies, in which $(\bar{n})$ retains most of the $\bar{p}$ energy similar to elastic collisions. This aspect has been examined [3] and the new $\sigma_{deepin}(E)$ cross-section is incorporated in this investigation.

The measurement of the atmospheric $\bar{p}$s was undertaken by the BESS Group [4] below a few GeV and results are now available at balloon and mountain altitudes. Theoretical estimate of the spectra of secondary $\bar{p}$s at large atmospheric depths can be directly compared with the measurements, as the primary spectrum gets depleted. At small atmospheric depths, they measured the $\bar{p}$ spectrum below the geomagnetic cut-off, where only a few tertiary $\bar{p}$ from primary $\bar{p}$ are present. Comparison of the calculated spectrum with the data re-assures the atmospheric corrections made in experiments and provides the validity of propagation models. In this investigation, three dimensional approach has been made in which propagation equations for different zenith angles have been solved simultaneously for primary nucleons and for both $(\bar{p})$ & $(\bar{n})$.

2. Cross-sections

The available cross-sections for different processes in $(\bar{p}, p)$ collisions were examined carefully and parameterized with a minimum number of parameters [3]. In Figure 1 is plotted the total inelastic cross-section, the difference between total and elastic cross- sections [5], multiplied by a factor 2 for convenience of plotting, by open circles as a function of kinetic energy E. This can be represented by the relation [3],

$$\sigma_{in}^{T}(\bar{p},p) = \sigma_T(\bar{p},p) - \sigma_{el}(\bar{p},p)$$
$$= 32.0[1.0 + 0.027\ln(\omega) + 0.01\ln^2(\omega)\theta(\omega) + 0.19\exp(-0.021E) + 0.79E^{-0.55}] \quad \text{mb} \qquad (1)$$

and is shown by Curve A. Here, $\omega = E/300$, $\theta(\omega) = 1.0$ for $E > 300GeV$ and = 0 for $E \leq 300GeV$.

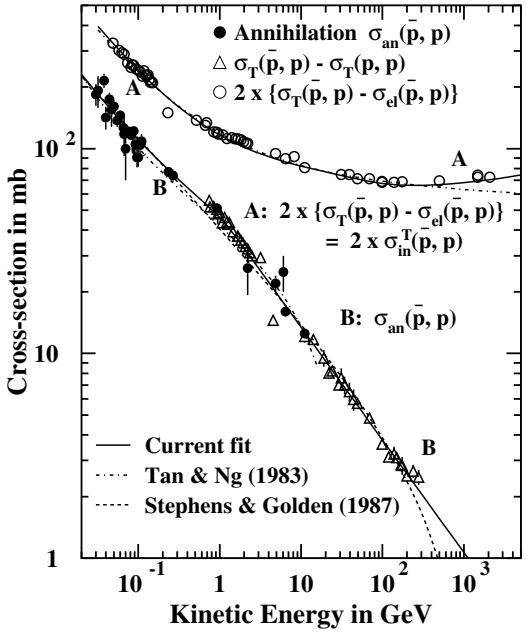

Figure 1. Curve A shows the total inelastic cross-section and Curve B the annihilation cross-sections for $\bar{p}$.

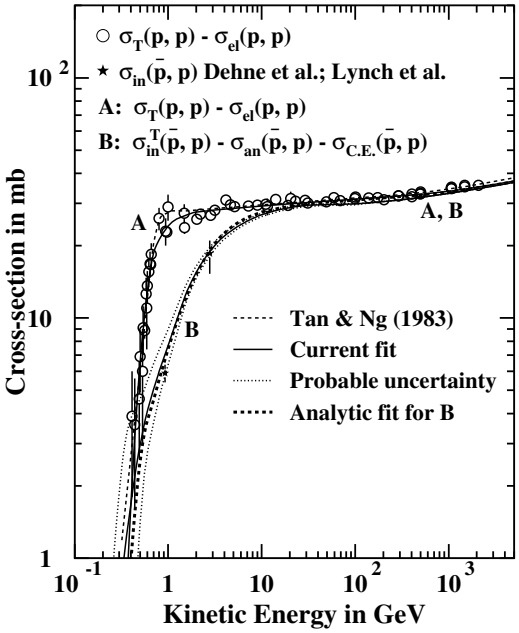

Figure 2. Curves A & B show the deep inelastic cross-sections for p and $\bar{p}$ without charge exchange process.

Direct measurement of the annihilation cross-section as a function of energy is shown in Fig.1 by solid circles and the open triangles are the difference between the total cross-sections $\sigma_T(\bar{p},p)$ and $\sigma_T(p,p)$ [6]. The solid line is the fit to the data and is represented by the relation [3],

$$\sigma_{an}(\bar{p},p) = 47.6E^{-0.55} \quad \text{mb} \quad \text{for } E > 1.2GeV \qquad (2a)$$
$$= 22.5[E^{-0.56} + 1.31\exp(-0.22E)] \quad \text{mb} \quad \text{for } E \leq 1.2GeV \qquad (2b)$$

The dashed curve is the fit given by Stephens and Golden [7] and the dash-dotted one is due to Tan and Ng [8].

The deep inelastic cross-section for $(\bar{p},p)$ interactions is the difference between the total inelastic cross-section $\sigma_{in}^{T}(\bar{p},p)$ and the sum of the annihilation and charge exchange $\sigma_{C.E}(\bar{p},p)$ cross-sections.This shown by the solid curve B in Fig.2. The thick dashed curve B is the fit adjusted to the data [9] and is given by [3]

$$\sigma_{Deepin}(\bar{p},p) = 32.0[1.0 + 0.027\ln(\omega) + 0.01\ln^2(\omega)\theta(\omega)]/f(E) \quad \text{mb} \qquad (3a)$$
$$= 21.24E^{2.5} - 1.0 \quad \text{mb} \qquad (3b)$$

where, $f(E) = 1.0 + 2.65E^{-1.7}$. The difference between total inelastic cross-section (Eqn.1) and the annihilation cross-section (Eqn.2) gives a large cross-section of about 20 mb below 2 GeV down to 100 MeV. It is important to mention that including this as part of deep inelastic cross-section is wrong.

3. 3-D Calculations

The method used in this calculation is similar to the one described earlier [1] except for updating the cross-sections and the changes required to incorporate 3-D effect. The propagation equation for the $\bar{p}$ is given by,

$$\frac{\partial(J_{\bar{p}}(E,x,\theta)}{\partial x} = Q_{\bar{p}}(E,x,\theta) + \frac{\partial}{\partial E}[J_{\bar{p}}(E,x,\theta)\frac{dE}{dx}] - \frac{J_{\bar{p}}(E,x,\theta)}{\Lambda(E)} + \Psi(E,x,\theta) \quad (4)$$

The first term in the R.H.S. is the production term, the second is the ionization term, third is the attenuation term, which includes annihilation and interaction, and the last term is the interaction term which produces tertiary $\bar{p}$s and $\bar{n}$s. This term above 15 GeV takes the form,

$$\Psi(E,x,\theta) = \int_q^0 \{J_{\bar{p}}(E/y,x,\theta)(1-\alpha) + J_{\bar{n}}(E/y,x,\theta)\alpha\}dy/\{qy\lambda(E/y)\} \quad (4a)$$

In the above expression, energy of the interacting $\bar{p}$ is $E' = E/y$, $q = 0.95$ is the cut-off value of y, determined from earlier work [1], $\alpha = 0.33$ is the charge exchange probability and λ the mean free path for deep inelastic collision. For below 15 GeV, in the absence of invariant cross-section, the following approach is made. For every value of E', integration was performed over the allowed transverse momentum of the outgoing particle, P_t. P_t determines the direction of the interacting particle, which rotates about the direction of the outgoing particle, and hence azimuthal integration was also performed. Thus,

$$\Psi(E,x,\theta) = \int_q^0 \frac{dy}{qy\lambda(E/y)} \left[\frac{\int_0^{\gamma_{max}} \exp(-P_t/P_0)dP_t \sin(\gamma)d\gamma \int_0^{2\pi} QF(E/y,x,\psi)d\phi}{2\pi \int_0^{\gamma_{max}} \exp(-P_t/P_0)dP_t \sin(\gamma)d\gamma}\right] \quad (4b)$$

Here, $QF = J_{\bar{p}}(E/y,x,\psi)(1-\alpha) + J_{\bar{n}}(E/y,x,\psi)\alpha$ and $\psi^2 = \mid \{\theta^2 + \gamma^2 - 2\gamma\theta\cos(\phi)\} \mid$. The integral over ϕ was limited to values of $\psi < \pi/2$, the horizon. The denominator is the weighted slid angle.

The propagation equations for nucleons are similar to Eqn. 4, except the ionization term is not needed for neutral particle. A set of similar equations are required for different components and at different zenith angles. Primary cosmic ray nucleons above 4 GeV/nucleon were first propagated in the atmosphere. The 3-D effect for nucleons comes from deep inelastic interactions in which the incoming particle changes its direction. This effect is found to be small at energies $\geq$ 15 GeV, where Eqn.4a was used, and Eqn.4b was used for $E < 15GeV$. The production spectrum of $\bar{p}$ could be calculated accurately by taking care of the particle spectra at all angles. $\bar{p}$ and $\bar{n}$ components at all zenith angles were simultaneously propagated. At 0.1 GeV a step length of 0.3 g/cm^2 was used, and at $E > 0.1$ GeV variable steps were adopted to save computing time.

4. Results and Inferences

In figure 3 are plotted the observed spectra by the BESS group below 3 GeV at 10.6 and 742 g/cm^2 along with the results from this computations; calculated spectrta are also shown at 994 g/cm^2 . The solid curves in the figure are with 3-D effect, while the dashed curves are without. It can be noticed that at small atmospheric depth, 3-D effect gives higher flux at low energies compared to unidirectional flux. This can be understood from Fig.4, in which the flux at all energies increase with zenith angle and considerable fraction of low energy particles comes from large zenith angles. This is not only because of large angular deviation of $\bar{p}$ from its original direction even with small Pt, but also due to large path length available for interactions. At large depths, flux decreases with zenith angles and as a result low energy flux gets depleted with 3-D effect.

It can also be seen from Fig. 3, that calculated spectrum at small depth is higher than the measured flux. This is because, I have used the global spectra for the primary nucleons, whose absolute flux is higher than the BESS spectrum and is slightly steeper. Use of the BESS spectrum will considerably reduce this difference and the spectrum at large depth will not be affected because of the flatter spectrum. At large depths, a small change in the absolute value of the interaction mean free path also changes the calculated spectrum. Higher

the interaction mean free path, larger the flux. I like to emphesize that, because of the sensitiveness of the calculated absolute spectrum at large depths with the spectral index and interaction mean free path, one needs to give more importance to the spectral shape than the absolute spectrum. Incorporating charge exchange interactions at low energies did not change the results because the loss of $\bar{p}$ due to this process $(\bar{p}, p) \rightarrow (\bar{n}, n)$ is nearly compensated by the process $(\bar{n}, n) \rightarrow (\bar{p}, p)$ as the number of target p and n nuclei are the same, and the secondary radiation has nearly equal number of $\bar{p}$s and $\bar{n}$s.

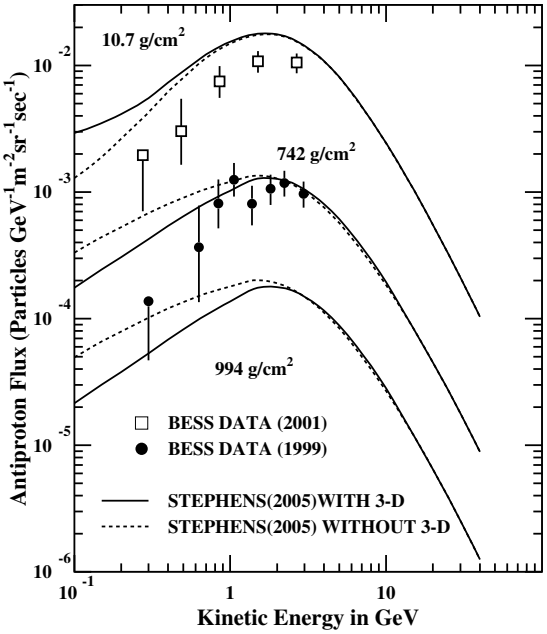

Figure 3. Calculated spectra are compared with the measurements at 2 depths. The dashed curves are without 3-D effect and the solid ones are with 3-D effect.

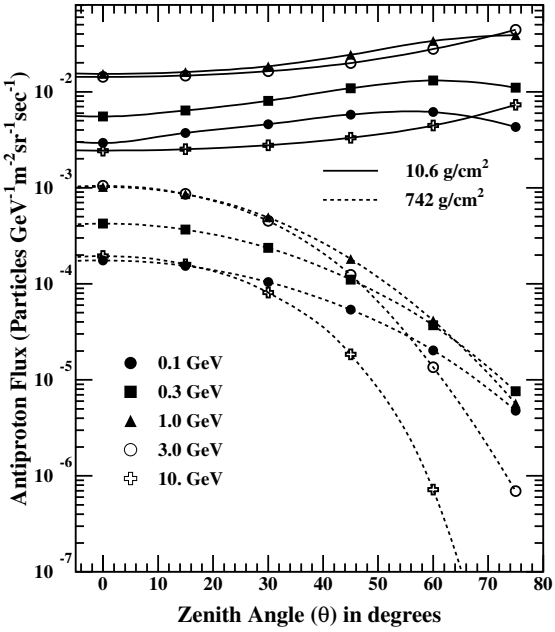

Figure 4. Zenith angle distribution of fluxes at 5 different energies are shown at depths 10.6 and 742 g/$cm^2$2.

References

[1] S.A.Stephens Astropart. Phys. 6, 229 (1997).
[2] C.Y. Huang et al., Phys. Rev. D68, 053008 (2003).
R. Duperray et al., Phys. Rev. D71, 083013 (2005).
[3] S.A. Stephens Advances in Sp. Res. 35, 142 (2005).
[4] K.Yamato et al., 28th ICRC, Tsukuba (2003) p. 1785.
T. Sanuki et al., Phys. Letters B577, 10 (2005).
[5] V. Flaminio et al.,Compilation of Cross-sections, p, $\bar{p}$ CERN-HERA 84-01 (1984).
K. Hagiwara et al., Phys. Rev. D66, 01001 (2002).
[6] J. Whitmore Phys. Reports 27C, 187 (1976).
[7] S.A. Stephens and R.L. Golden Sp. Sci. Rev. 46, 31 (1987).
[8] L.C. Tan and L.K. Ng J. Phys. G9, 227 and 1289 (1983).
[9] H.C. Dehne et al., Phys. Rev. 136B, 843(1964).
R.R. Lynch et al., Phys. Rev. 131, 1276 (1963).